Dalton Transactions

ROYAL SOCIETY OF CHEMISTRY

PAPER

View Article Online
View Journal | View Issue

Check for updates

Cite this: *Dalton Trans.*, 2026, **55**, 4237

Nicotinoyl hydrazone-directed vanadium assemblies: metallosupramolecular isomerism, polymorphism, and catalytic oxidation performance

Edi Topić, Josipa Sarjanović, Dino Kuzman, Andrea Cocut, Tomica Hrenar, Jana Pisk * and Višnja Vrdoljak *

A systematic investigation of coordination-driven vanadium assemblies reveals a rich structural landscape in which tetrameric metallacycles $[VO(VanNH)(OR)]_4$ and 1D polymeric species $[VO(VanNH)(OR)]_n$ form selectively, depending on reaction conditions and the nature of auxiliary alkoxide ligands (VanNH = *o*-vanillin nicotinoylhydrazone; R = C_nH_{2n+1}, n = 1–5). Additionally, several polymorphs and structural isomers are identified, along with a rare reversible, temperature-dependent phase transformation. The assemblies can be classified into three distinct structural types based on the intramolecular orientation of the pyridyl moieties: (i) type I featuring alternating '*syn*'/'*anti*' arrangements, (ii) type II with a uniform '*anti*' motif, and (iii) type III composed exclusively of '*syn*' units. Quantum-chemical calculations reveal that polymers adopting the alternating '*syn*'/'*anti*' motif are thermodynamically most stable, primarily due to more exothermic enthalpies of formation. In contrast, polymeric structures dominated by '*anti*' arrangements become favored for longer alkoxo ligands, whereas the tetranuclear metallocycles exhibit only modest stabilization across the alkoxide series. The pronounced structural diversity arises from a subtle interplay among electronic, steric, and crystal-packing effects that governs phase selection and crystallization behavior. In the catalytic oxidation of Cl- and NO_2-substituted benzyl alcohols using *tert*-butyl hydroperoxide (TBHP), the tetranuclear complexes initially exhibit high selectivity toward aldehyde formation, while the polymeric species achieve superior overall conversion. The results highlight a fundamental trade-off between catalytic activity and selectivity, strongly modulated by catalyst nuclearity and alkoxo ligand length. The insights gained provide valuable design principles for developing vanadium-based assemblies with tunable properties.

Received 27th December 2025,
Accepted 17th February 2026

DOI: 10.1039/d5dt03088a

rsc.li/dalton

Open Access Article. Published on 17 February 2026. Downloaded on 4/5/2026 6:35:39 AM.
This article is licensed under a Creative Commons Attribution-NonCommercial 3.0 Unported Licence.

Introduction

Vanadium stands out among transition metals because of its accessible oxidation states, pronounced redox activity, and flexible coordination geometries.[1–4] These properties have facilitated the use of vanadium complexes in various chemical transformations, particularly oxidation reactions. The oxophilic nature of vanadium, particularly in its higher oxidation states (V^{IV} and V^{V}), promotes the activation of oxidants such as H_2O_2 and *tert*-butyl hydroperoxide (TBHP) for converting a wide range of substrates. Consequently, vanadium compounds are extensively studied for catalytic hydrocarbon oxidation,[5,6] oxidative dehydrogenation,[7] oxidative coupling reactions,[8] and asymmetric oxidations.[9] Additionally, their relatively low toxicity and versatile coordination chemistry make them appealing candidates for bioinorganic chemistry, materials science, and the development of functional materials.[10–13]

The ligand environment plays a crucial role in stabilizing vanadium oxidation states and influencing its catalytic behavior.[14,15] Through electronic donation, steric effects, and chelating geometry, hydrazone ligands can fine-tune the redox properties of the vanadium center, thereby influencing the accessibility and stability of higher oxidation states (V(IV), V(V)). These factors, in turn, directly affect the efficiency, selectivity, and mechanistic pathways of vanadium-catalyzed reactions.

Recent studies highlight the effectiveness of vanadium–hydrazone systems in selective oxidations. For instance, H. Hosseini Monfared *et al.* reported a silica-anchored oxovanadium(V) aroylhydrazone complex capable of hydrocarbon oxidation with H_2O_2, achieving turnover frequencies above 2500 h^{-1}.[16] More recently, oxovanadium(V) metallosupra-

University of Zagreb, Faculty of Science, Department of Chemistry, Horvatovac 102a, 10000 Zagreb, Croatia. E-mail: visnja.vrdoljak@chem.pmf.hr, jana.pisk@chem.pmf.hr

Open Access Article. Published on 17 February 2026. Downloaded on 4/5/2026 6:35:39 AM.
This article is licensed under a Creative Commons Attribution-NonCommercial 3.0 Unported Licence.

molecular complexes with isonicotinoylhydrazonate ligands efficiently catalyzed the oxidation of benzyl alcohol and its derivatives using TBHP or H_2O_2, achieving over 80% conversion with high selectivity under mild conditions.[17,18] The main challenge in this reaction is maintaining high selectivity for benzaldehyde and avoiding over-oxidation to benzoic acid, especially under green or mild conditions.[19]

When coordinated with hydrazone ligands, vanadium readily forms stable and structurally diverse complexes. Nevertheless, the structural landscape of vanadium-based metallosupramolecular systems, particularly regarding isomerism and polymorphism, remains insufficiently explored. To address this, we focused on hydrazone ligands featuring nicotinoyl groups, selected for their capacity to chelate metal centres and to support metallosupramolecular structure assembly.[19–21] Specifically, we employed the {VO(VanNH)} structural unit (Scheme 1), derived from the *o*-vanillin nicotinoylhydrazonato ligand ($VanNH^{2-}$), in combination with various alkoxides (RO^-). The ligand bridges vanadium centers, facilitating the formation of either discrete metallocyclic tetranuclear species $[VO(VanNH)(OR)]_4$, or extended polymeric assemblies $[VO(VanNH)(OR)]_n$.

However, the same building blocks can self-assemble in different ways, resulting in various possible outcomes. They depend on differences in ligand orientation, or network topology, and are influenced by subtle variations in reaction conditions.[22–24] Gaining a fundamental understanding of the parameters that influence such divergent assembly outcomes is therefore essential for the rational design of functional materials within this class. To accomplish this, we used quantum-chemical calculations to compare the relative thermodynamic stabilities of cyclic tetrameric architectures and extended polymeric structures of various types.

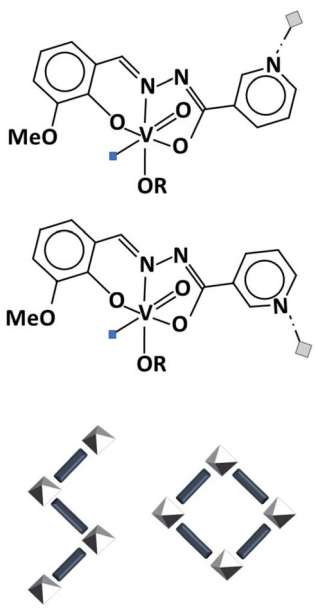

Scheme 1 Schematic representation of the {VO(VanNH)(OR)} with '*anti*' (top) or/and '*syn*' (middle) arrangements of building units in polymeric and metallocyclic assemblies. R corresponds to CH_3, C_2H_5, C_3H_7, $CH(CH_3)_2$, C_4H_9, $C(CH_3)_3$, and C_5H_{11}. Grey squares denote potential positions of vanadium centres within the resulting metallosupramolecular assemblies, while blue squares indicate potential nitrogen donor atoms.

Although polymorphism has been observed in neutral vanadium complexes spanning oxidation states III to V, particularly those incorporating hydrazones,[25–29] Schiff bases,[30–32] and pyridine derivatives,[33,34] such phenomena typically occur in systems lacking strong directional interactions. A notable example is the vanadium(IV) porphyrin complex V(O)TMeOPP, which undergoes a reversible, temperature-dependent phase transformation between two polymorphs, driven by subtle changes in supramolecular packing and weak hydrogen bonding.[35]

Variations in supramolecular arrangement and crystal packing within these architectures can lead to distinct physical and functional properties. In particular, bulky alkoxide ligands are known to hinder close molecular packing, often promoting the formation of more open frameworks with larger void volumes.[18] These structural features can directly affect diffusion pathways and, consequently, the catalytic performance of the resulting assemblies.

To evaluate their catalytic activity, the complexes were tested in the oxidation of 4-chlorobenzyl alcohol and 4-nitrobenzyl alcohol to the corresponding aldehydes, using aqueous *tert*-butyl hydroperoxide (TBHP) as a green and efficient oxidant. For comparison, the catalytic behavior of $[VO(acac)_2]$ and $(NH_4)VO_3$ was also assessed under identical conditions. This comparative approach allowed for a systematic analysis of how ligand structure and coordination environment influence both catalytic efficiency and selectivity, providing useful design principles for developing more effective and sustainable oxidation catalysts.

Results and discussion

Synthesis and structural characterization of vanadium assemblies

The hydrazone derived from *o*-vanillin and nicotinoylhydrazide (H_2VanNH) was synthesized following literature procedures.[36] A series of vanadium-based metallosupramolecular coordination compounds was then prepared by reacting NH_4VO_3 or $[VO(acac)_2]$ with H_2VanNH in the presence of various alcohols ($C_nH_{2n+1}OH$, n = 1–5), as outlined in Table 1.

High-quality crystals of **1**, **2**, **3t**, **3α**, **3β**, **3t^{iso}**, **4α**, **4β**, **4^{tert}**, **5tα**, and **5tβ** were analysed with single-crystal X-ray diffraction, and their crystal structures were determined (Table S1, see SI). Across the series, each oxovanadium(V) center adopts the expected pseudooctahedral *ONO* coordination from the doubly deprotonated $VanNH^{2-}$ ligand in its enolato-imino tautomeric form, while the remaining sites are occupied by an alkoxide ligand and a pyridyl nitrogen that enables the interconnection of monomeric units (Fig. 1, top). Selected bond metrics (Fig. S2, see SI) show a highly conserved first coordination sphere, consistent with this assignment.

This journal is © The Royal Society of Chemistry 2026

Open Access Article. Published on 17 February 2026. Downloaded on 4/5/2026 6:35:39 AM.
This article is licensed under a Creative Commons Attribution-NonCommercial 3.0 Unported Licence.

Table 1 Metallosupramolecular isomers and polymorphic forms obtained from different alcohols

Comp.	Solvent	Formula
1	Methanol	$[VO(VanNH)(OCH_3)]_n$
2	Ethanol	$[VO(VanNH)(OCH_2CH_3)]_n$
3t	*n*-Propanol	$[VO(VanNH)(OC_3H_7)]_4$
3α	*n*-Propanol	$[VO(VanNH)(OC_3H_7)]_n$
3β	*n*-Propanol	$[VO(VanNH)(OC_3H_7)]_n$
3t^{iso}	Isopropanol	$[VO(VanNH)\{OCH(CH_3)_2\}]_4$
4α	*n*-Butanol	$[VO(VanNH)(OC_4H_9)]_n$
4β	*n*-Butanol	$[VO(VanNH)(OC_4H_9)]_n$
4^{tert}	*tert*-Butanol	$[VO(VanNH)\{OC(CH_3)_3\}]_n$
5tα	*n*-Pentanol	$[VO(VanNH)(OC_5H_{11})]_4$
5tβ	*n*-Pentanol	$[VO(VanNH)(OC_5H_{11})]_4$

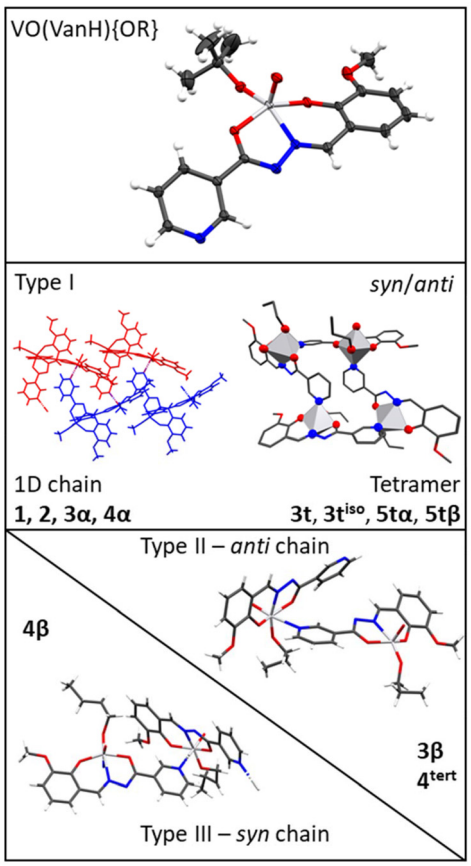

Fig. 1 Top: A molecular structure of a representative monomeric unit (as found in **3t^{iso}**). Middle: Diagrams of 1D polymeric chains (left) and tetramers (right) for polymeric type I. In polymeric chains, consecutively connected '*syn*'/'*anti*' dimers are coloured differently. In tetramers, hydrogen atoms are omitted for clarity. Bottom: Examples of polymeric types II and III are shown as two connected monomers.

Reactions involving small alkoxide ligands, such as methoxide and ethoxide, consistently resulted in the formation $[VO(VanNH)(OCH_3)]_n$ (**1**) and $[VO(VanNH)(OCH_2CH_3)]_n$ (**2**). They crystallize as one-dimensional (1D) coordination polymers in the space group $P2_1/c$.

As the alkoxide groups became bulkier, interesting structural diversities were observed (Table 1). Specifically, the use of *n*-propanol led to the formation of both a discrete tetranuclear metallacycle, $[VO(VanNH)(OC_3H_7)]_4$ (**3t**), and a polymorphic pair of chain polymers $[VO(VanNH)(OC_3H_7)]_n$ (**3α** and **3β**). They crystallize in the space group $P\bar{1}$, *Pbca*, and $Pna2_1$, respectively. Complex **3t** is formed as the only product when $[VO(acac)_2]$ serves as the starting material. In contrast, when ammonium vanadate is employed, the formation of the tetramer **3t** along with polymorphs, **3α** and **3β** is possible, depending on the reaction or crystallization conditions. If these conditions are not carefully optimized, these compounds may crystallize concomitantly.

This coexistence of structurally distinct species highlights the sensitivity of metallosupramolecular isomerism and polymorphism to synthetic parameters such as solvent, concentration, and crystallization conditions. Similarly, the isopropoxide derivative, $[VO(VanNH)\{OCH(CH_3)_2\}]_4$ (**3t^{iso}**), was obtained exclusively as a discrete tetramer. This preference is attributed to the increased steric hindrance imposed by the alkoxide group.

Repeated attempts to isolate discrete cyclic species with either *n*-butoxyde or *tert*-butoxyde ligands were unsuccessful under the investigated conditions. Instead, these co-ligands consistently yielded one-dimensional polymeric structures $[VO(VanNH)(OC_4H_9)]_n$ (**4α** ($P2_1/c$), **4β** ($R\bar{3}$), for *n*-butoxide, and **4^{tert}** (*Fdd*2) for *tert*-butoxide).

Interestingly, for the *n*-pentoxide derivative, two tetrameric polymorphs, $[VO(VanNH)(OC_5H_{11})]_4$ (**5tα** and **5tβ**) with $P\bar{1}$ symmetry were identified (at 170 K and at RT). They interconvert reversibly with temperature changes, with **5tα** being the low-temperature form. These conformers exhibit subtle structural differences, underscoring the pronounced thermal and structural adaptability of the metallosupramolecular architectures.

The content of the asymmetric units reveals pronounced conformational diversity: except for the high-symmetry structures **4β** and **4^{tert}**, all crystals contain more than one independent monomeric unit ($Z' > 1$, see SI, Fig. S2), which can be ascribed to monomer flexibility and conformational disorder of the alkoxide ligands. Such behavior is well known to accompany packing frustration in molecular crystals, and recent analyses of high-Z' structures might extend this interpretation to metallo–organic assemblies.[37]

The presence of multiple symmetrically inequivalent monomeric units is a consequence of multiple orientations of pyridyl fragments needed to build the polymeric species. Still, the condition is not present in all of the structures. Herein, we will define the orientation of the pyridyl nitrogen atom towards the hydrazonato oxo group in the same monomer as '*syn*', and opposite orientation as '*anti*' (Scheme S1, see SI). Most of the structures, including cyclic tetramers and polymers (**1**, **2**, **3α**, **3t**, **3t^{iso}**, **4α**, **5tα**, and **5tβ**), conform to type I arrangement and show alternating '*syn*'/'*anti*' orientations in neighbouring monomeric units (Fig. 1, middle). However, the structures of **3β** and **4^{tert}**, classified as polymeric type II, show only '*anti*' orientations, whereas the structure of **4β** (polymeric type III) shows only '*syn*' orientations (Fig. 1, bottom).

Open Access Article. Published on 17 February 2026. Downloaded on 4/5/2026 6:35:39 AM.
This article is licensed under a Creative Commons Attribution-NonCommercial 3.0 Unported Licence.

The 1D chains in **1**, **2**, **3α**, **3β**, **4α**, **4β**, and $\mathbf{4}^{tert}$ are constructed by V–pyridyl–N coordination bonds into linear, uninodal nets that can be described by the ubiquitous 2C1 topology (two-connected 1D net). Densities extrapolated to 170 K (see SI, Fig. S3–S5) show that **α** polymorphs pack more efficiently than **β** forms. The void volumes are generally small, indicating dense packing across the series.

The polymorphism observed in **3** and **5**, albeit rarely encountered in metal–organic polymers, is expected for conformationally flexible monomeric units and often arises in systems lacking strong directional hydrogen bonds, which is precisely the case here, where deprotonation removes classical donors, and packing is governed by weak contacts. Representative studies document polymorphism, concomitant crystallization, and solid-state transformations in both polymers and MOFs, providing precedents for the observation of α/β pairs.[38]

Additional features worth noting include the slight but systematic increase of void volume with alkyl chain length (yet remaining negligible in absolute terms), and the absence of strong hydrogen bonding across all structures. Both observations are consistent with densely packed vanadium–hydrazonato frameworks stabilized by numerous weak C–H···O contacts rather than specific supramolecular synthons.

Overall, the crystallographic landscape – conserved *ONO* coordination, frequent $Z' > 1$ as a consequence of pyridyl fragment orientation, chain/tetramer isolation based roughly on auxiliary ligand choice, α/β polymorphism of chains – paints a coherent picture of a flexible {VO(VanNH)(OR)} building unit exploring a narrow conformational space between discrete and polymeric assemblies.

Quantum chemical calculations

To gain deeper insights into the factors driving the formation of distinct structural isomers, extensive quantum chemical calculations were performed. The stability of tetrameric complexes was analyzed using experimental structures, which were subjected to geometry optimizations and harmonic frequency calculations. For complexes for which experimental structures were unavailable, equivalent geometries were generated for calculations. Standard Gibbs binding energies for tetramer models were calculated by subtracting the energy of four monomers, each with the pyridine molecule occupying the sixth coordination site, from the tetramer energy. Labels '*syn*' and '*anti*' refer to the monomer in which the nitrogen atom of the nicotinoyl moieties is oriented towards the oxo group and opposite to the oxo group, respectively (Fig. 2 and 3).

$$\Delta_b G^\circ(\text{tetramer, cycle}) = \Delta_f G^\circ(\text{tetramer, cycle}) - 2\Delta_f G^\circ_{syn}(\text{monomer, py}) - 2\Delta_f G^\circ_{anti}(\text{monomer, py}) + 4\Delta_f G^\circ(\text{py}) \quad (1)$$

Based on the calculated standard Gibbs binding energies (eqn (1), Table 2), the formation of cyclic tetramers over monomers is predicted to be thermodynamically favorable for all investigated structures.

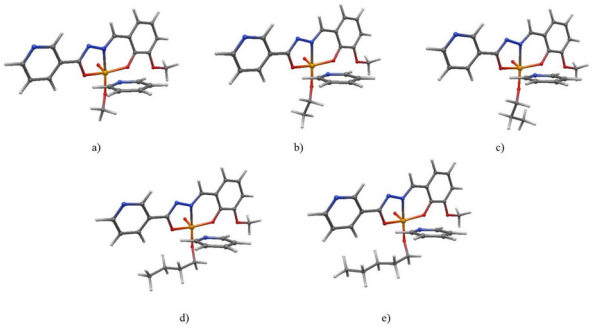

Fig. 2 Optimized monomer geometries with the $VanNH^{2-}$ ligand and the pyridine nitrogen atom directed opposite to the oxo groups at the B3LYP-D3BJ/6-31G(d) level of theory. The structures are ordered by the increasing length of the alkyl chain (R = C_nH_{2n+1}, n = 1–5).

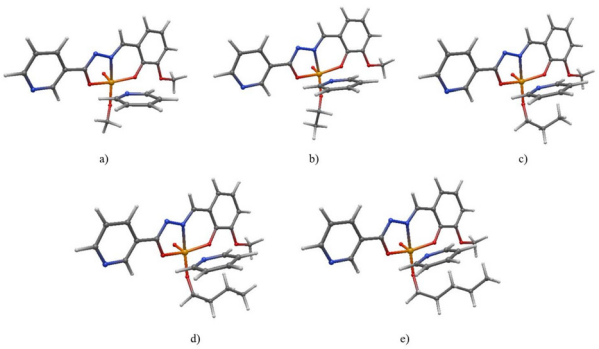

Fig. 3 Optimized geometries of monomers with $VanNH^{2-}$ ligand and pyridine nitrogen atom oriented towards oxo groups at B3LYP-D3BJ/6-31G(d) level of theory. Structures are ordered by increasing alkyl chain length (R = C_nH_{2n+1}, n = 1–5).

Table 2 Standard enthalpies, entropies and Gibbs binding energies of tetrameric cycle structures compared to monomeric ones calculated using density functional theory at the B3LYP-D3BJ/6-31G(d) level of theory (at T = 298.15 K and p = 101 325 Pa)

Ligand	$\Delta_b H°$/kJ mol^{-1}	$\Delta_b S°$/J K^{-1} mol^{-1}	$\Delta_b G°$/kJ mol^{-1}
$-OCH_3$	−92.06	19.57	−97.89
$-OC_2H_5$	−115.45	−33.43	−105.49
$-OC_3H_7$	−93.49	18.16	−98.90
$-OC_4H_9$	−84.20	53.53	−100.16
$-OC_5H_{11}$	−73.20	55.10	−89.63

To further evaluate tetramer stability, additional calculations were performed using chain-tetramer models. For each ligand, a tetranuclear chain was constructed with the sixth coordination site of the terminal metal center occupied by a pyridine molecule, ensuring a consistent coordination environment across all models. Due to the possibility of different assembly motifs, two tetrameric chain structures are considered: type I, with alternating '*syn*' and '*anti*' building blocks, and type II, which features only '*anti*'-oriented structural units. The standard Gibbs binding energies of these tet-

 This journal is © The Royal Society of Chemistry 2026

Open Access Article. Published on 17 February 2026. Downloaded on 4/5/2026 6:35:39 AM. This article is licensed under a Creative Commons Attribution-NonCommercial 3.0 Unported Licence.

ramers, compared to their respective monomers, were then calculated.

$$\Delta_b G_I^\circ(\text{tetramer, chain}) = \Delta_f G_I^\circ(\text{tetramer, chain}) - 2\Delta_f G_{syn}^\circ(\text{monomer, py}) - 2\Delta_f G_{anti}^\circ(\text{monomer, py}) + 3\Delta_f G^\circ(\text{py}) \quad (2)$$

$$\Delta_b G_{II}^\circ(\text{tetramer, chain}) = \Delta_f G_{II}^\circ(\text{tetramer, chain}) - 4\Delta_f G_{anti}^\circ(\text{monomer, py}) + 3\Delta_f G^\circ(\text{py}) \quad (3)$$

It was found that the first chain assembly type (Table 3) is more stable than the second (Table 4). This is supported by the consistently more negative $\Delta_b G_I^\circ$ calculated for the alternate arrangement, indicating an increasing overall driving force for polymer assembly. The higher stability of type I chain mainly arises from its notably more exothermic binding enthalpies ($\Delta_b H^\circ$), which compensate for the entropic effects involved in polymer assembly.

Conversely, the '*anti*' chain type (Table 4) is characterized by a systematically more negative $\Delta_b S_{II}^\circ$. This reduces the overall thermodynamic favorability of this chain type II, particularly for shorter alkoxy co-ligands. However, for longer alkoxides like $-OC_4H_9$ and $-OC_5H_{11}$, the '*anti*' motif becomes more favorable due to the total constant entropy contribution within the series. The chain model with all '*syn*' orientations was not included in the calculations, as it is obtained in only one polymeric structure, **4β**.

The difference in standard Gibbs energies of formation of cyclic tetramers compared to chains of the corresponding length. $\Delta\Delta_f G^\circ$(tetramer, cycle – tetramer, chain) was calculated as

$$\Delta\Delta_f G^\circ(\text{tetramer, cycle} - \text{tetramer, chain}) = \Delta_f G^\circ(\text{tetramer, cycle}) - \Delta_f G^\circ(\text{tetramer, chain}) + \Delta_f G^\circ(\text{py}) \quad (4)$$

The results indicate that the chain structures with alternating '*syn*' and '*anti*' building units are not only thermodynamically more stable than the '*anti*' chain type, but also more stable than their corresponding cyclic tetramers across the examined alkoxy series (Tables 5 and 6). The cyclic tetramers offer modest enthalpy stabilization, making them less stable as the alkoxy-ligand size becomes larger.

An interesting outlier in the series is the absence of tetrameric assembly for complexes derived from the *n*-butoxide ligand, whereas such assemblies were isolated for the *n*-propoxide, isopropoxide, and *n*-pentoxide ligands. However, in this series, there are certainly multiple interactions in a delicate balance – packing efficiency, alkoxide chain setting, position of the pyridyl nitrogen atom, slight variations in ligand conformation, and small differences in solubility, which together might force the crystallization into (only) one type of network. A detailed understanding of this behaviour would require significant additional data in both the chemical and external parameter domains (*e.g.* temperature or moisture level).

PXRD

Although slight changes in reaction conditions and auxiliary alkoxide ligands affect the resulting structures, all complexes were obtained in pure form. Crystalline powders were analysed

Table 3 Standard enthalpies, entropies and Gibbs binding energies of tetrameric chain structures, type I, with alternating '*syn*' and '*anti*' building units compared to monomers calculated using density functional theory at the B3LYP-D3BJ/6-31G(d) level of theory (at T = 298.15 K and p = 101 325 Pa)

Ligand	$\Delta_b H_I^\circ$/kJ mol^{-1}	$\Delta_b S_I^\circ$/J K^{-1} mol^{-1}	$\Delta_b G_I^\circ$/kJ mol^{-1}
$-OCH_3$	−157.07	−193.12	−99.49
$-OC_2H_5$	−176.75	−224.41	−109.84
$-OC_3H_7$	−188.24	−223.62	−121.57
$-OC_4H_9$	−185.43	−190.39	−128.67
$-OC_5H_{11}$	−191.34	−194.55	−133.33

Table 4 Standard enthalpies, entropies, and Gibbs binding energies of tetrameric chain structures, type II, with '*anti*'-oriented structural units compared to monomers calculated using density functional theory at the B3LYP-D3BJ/6-31G(d) level of theory (at T = 298.15 K and p = 101 325 Pa)

Ligand	$\Delta_b H_{II}^\circ$/kJ mol^{-1}	$\Delta_b S_{II}^\circ$/J K^{-1} mol^{-1}	$\Delta_b G_{II}^\circ$/kJ mol^{-1}
$-OCH_3$	−131.95	−215.65	−67.65
$-OC_2H_5$	−142.53	−239.20	−71.21
$-OC_3H_7$	−159.38	−242.34	−87.13
$-OC_4H_9$	−176.02	−209.46	−113.57
$-OC_5H_{11}$	−191.34	−219.79	−125.81

Table 5 Relative standard enthalpies, entropies and Gibbs formation energies of tetrameric cyclic structures compared to the chain type I structures calculated using density functional theory at the B3LYP-D3BJ/6-31G(d) level of theory (at T = 298.15 K and p = 101 325 Pa)

Ligand	$\Delta\Delta_f H^\circ$/kJ mol^{-1}	$\Delta\Delta_f S^\circ$/J K^{-1} mol^{-1}	$\Delta\Delta_f G^\circ$/kJ mol^{-1}
$-OCH_3$	65.01	212.69	1.59
$-OC_2H_5$	61.29	190.98	4.35
$-OC_3H_7$	94.75	241.78	22.67
$-OC_4H_9$	101.23	243.92	28.50
$-OC_5H_{11}$	118.14	249.65	43.71

Table 6 Relative standard enthalpies, entropies and Gibbs formation energies of tetrameric cyclic structures compared to the chain type II structures calculated using density functional theory at the B3LYP-D3BJ/6-31G(d) level of theory (at T = 298.15 K and p = 101 325 Pa)

Ligand	$\Delta\Delta_f H^\circ$/kJ mol^{-1}	$\Delta\Delta_f S^\circ$/J K^{-1} mol^{-1}	$\Delta\Delta_f G^\circ$/kJ mol^{-1}
$-OCH_3$	40.22	233.90	−29.52
$-OC_2H_5$	27.25	204.17	−33.62
$-OC_3H_7$	56.39	228.79	−11.83
$-OC_4H_9$	86.42	261.71	8.39
$-OC_5H_{11}$	108.39	265.66	29.18

Open Access Article. Published on 17 February 2026. Downloaded on 4/5/2026 6:35:39 AM.
This article is licensed under a Creative Commons Attribution-NonCommercial 3.0 Unported Licence.

using the powder X-ray diffraction (PXRD) method, and their experimental patterns were compared to simulated diffractograms derived from single-crystal X-ray diffraction (SCXRD) data. In all cases, the PXRD patterns matched the corresponding simulated diffractograms, confirming phase purity and the absence of polymorphic or isomeric impurities (Fig. S6, see SI).

ATR-IR spectra

The infrared spectra of the synthesized complexes showed clear evidence of ligand coordination through the disappearance of characteristic vibrational bands associated with the free hydrazone ligand. Specifically, the O–H (3300 cm^{-1}), C═O (1671 cm^{-1}), and N–NH (3186 cm^{-1}) stretching bands were no longer observed upon complexation with vanadium (Fig. S7 and S8, SI). Their disappearance was accompanied by the emergence of new absorption features, confirming coordination *via* both oxygen- and nitrogen-donor atoms. Notably, bands observed near 1610 cm^{-1} ($C{=}N_{imine}$), 1350 cm^{-1} ($C{-}O_{hydrazonato}$), and 1255 cm^{-1} ($C{-}O_{phenolic}$) confirmed metal–ligand binding *via* the hydrazone backbone.

Further support for complex formation came from weaker-intensity metal–ligand vibrations, including bands at approximately 740 cm^{-1} ($V{-}N_{imine}$), 590 cm^{-1} ($V{-}O_{hydrazonato}$), and 580 cm^{-1} ($V{-}O_{phenolato}$). A moderate-intensity band around 1610 cm^{-1} was assigned to the C═N stretch of the nicotinoyl pyridine moiety. Its shift to a lower wavenumber compared to the free ligand indicated coordination of the pyridine nitrogen to the $\{VO\}^{3+}$ core. Additionally, a distinct band at near 970 cm^{-1} was attributed to N–N vibrations, while a medium-intensity band around 720 cm^{-1} was consistent with V–N stretching, further supporting metallosupramolecular assembly.

The coordination of the alkoxide group was evidenced by the appearance of a new absorption band near 1030 cm^{-1}, typical for $C{-}O_{OR}$ stretches. Slight variations in this region across complexes reflect differences among the coordinated alcohols relative to their free forms. All complexes in the series exhibited intense bands near 960 cm^{-1} range, characteristic of the $\{VO\}^{3+}$ oxo-core.

Additionally, differences observed in the spectral features of complexes reflect variations in overall molecular and crystal architectures. These differences are consistent with the formation of polymorphic forms or metallosupramolecular isomers, likely arising from variations in packing, hydrogen bonding, and the spatial arrangement of coordinating ligands and alkoxide groups within the assemblies.

NMR spectra

In CD_3OD solution, the ^1H NMR spectra of vanadium compounds exhibited a well-defined set of signals, consistent with ligand coordination (Scheme S2, Table S2, Fig. S9 and S10 see SI). The azomethine proton (H1) exhibited a notable downfield shift of 0.22 ppm compared to the free ligand, indicative of coordination to the vanadium center. In contrast, only subtle chemical shift changes were observed for the nicotinoyl protons: H8, H9 and H10 shifted slightly upfield, while H6 exhibited a minor downfield shift. These observations suggest that, in dilute methanolic solution, the pyridine nitrogen of the nicotinoyl group is not coordinated to the metal center. Additionally, the ^1H and ^{13}C NMR spectra exhibit a single, well-defined set of ligand-based resonances with narrow lines. If chain or tetranuclear structures were preserved, broadened signals would be expected due to different assembly motifs. Therefore, NMR data suggest that, in diluted CD_3OD solutions, the oligomeric framework disassembles and mononuclear, solvated complexes form, rather than preserving the original tetrameric or polymeric structure.

The aromatic region of the spectrum provided further confirmation of coordination. Protons H14 and H16 appeared as doublets of doublets, while H15 was observed as a triplet with a noticable upfield shift, reflecting changes in the electronic environment induced by metal coordination. The overall spectral features were generally consistent across the series of vanadium compounds. All complexes displayed very similar spectra (Fig. S11, see SI), chemical shift values, and multiplicities for the ligand-derived resonances, confirming that the metal–hydrazone complex unit is preserved in solution. The only noticeable differences among the spectra arose from additional resonances attributable to residual free alcohols, whose nature depended on the originally coordinated alkoxo ligand (RO). This observation suggests that upon dissolution of the complexes in CD_3OD, the ancillary RO ligand is readily replaced by CD_3O^-, thereby releasing the corresponding free alcohol into solution. Such solvent-induced ligand exchange is consistent with the lability of alkoxo ligands in protic solvents,[39] such as alcohols, and is in good agreement with our previous findings.[17] Unfortunately, the low solubility of all investigated compounds prevented a detailed NMR analysis in non-coordinating solvents.

The ^{13}C NMR spectra further supported ligand coordination, revealing significant deshielding for carbon atoms in proximity to the coordination sites (Table S2 and Fig. S10, see SI). In particular, carbons C1, C4, and C12 exhibited pronounced downfield shifts of up to 3.77 ppm, 6.91 ppm, and 7.35 ppm, respectively. In contrast, the carbon atoms of the nicotinoyl ring (C6–C10) showed minimal chemical shift changes ($\Delta\delta \leq 1$ ppm), supporting the conclusion that the pyridine nitrogen does not remain coordinated under the studied conditions.

Thermogravimetric analyses

The thermal stability of all assemblies was also investigated, revealing a consistent two-step decomposition process (Fig. S12, see SI). The initial mass loss, attributed to the oxidation of alkoxide groups, commenced within the temperature range of 142 °C to 181 °C, respectively, indicating improved thermal stability of the alkoxide ligands within the polymeric frameworks. The lowest oxidation onset temperatures were observed for the tetrameric complexes $\mathbf{3t^{iso}}$ and **5tβ**, at 146 °C and 142 °C, respectively. In contrast, the highest thermal stability was found for polymers **1** and **2**, with onset temperatures

 This journal is © The Royal Society of Chemistry 2026

Open Access Article. Published on 17 February 2026. Downloaded on 4/5/2026 6:35:39 AM. This article is licensed under a Creative Commons Attribution-NonCommercial 3.0 Unported Licence.

of 181 °C and 173 °C, respectively, corresponding to the oxidation of methoxy and ethoxy co-ligands, respectively. These mass losses are consistent with the release of aldehyde fragments, in line with previously reported thermal decomposition pathways of alkoxo-vanadium(v) complexes.[18,40] The second step involved decomposing the hydrazone ligands, occurring between 227 °C and 318 °C. In all cases, the final residues clearly indicated the formation of vanadium pentoxide, as confirmed by the residual mass percentages.

Catalytic performance

The catalytic study involved vanadium-based complexes bearing various coordinated alkoxo ligands, alongside NH_4VO_3 and [VO(acac)$_2$] as two independent reference systems. The substrates tested were 4-chlorobenzyl alcohol and 4-nitrobenzyl alcohol, with TBHP in water serving as the oxidizing agent. Due to the limited solubility of the aldehyde obtained from 4-chlorobenzyl alcohol substrate, 3 mL of acetonitrile was added to the reaction mixture as a co-solvent. All catalysts were classified as molecular ones based on their solubility in the reaction medium. Although 0.5 mol% of each catalyst was introduced in all reactions, the complexes exhibit different dissolution rates and extents in the reaction medium; therefore, the effective concentration of catalytically active species in solution may differ, which can contribute to the observed variations in catalytic activity. The reactions were monitored over a 2-hour period, and the results are summarized in Tables 7 and 8.

The catalytic performance in the oxidation of 4-chlorobenzyl alcohol to 4-chlorobenzaldehyde highlights catalysts **3**, **4**, and **4**^{tert}, all polymeric in nature, as the most effective in terms of conversion after 2 hours of reaction. These catalysts achieved conversion values of 79, 77, and 74%, respectively. However, when assessing catalyst activity at an earlier stage (after 20 minutes), catalysts **3** and **4** showed moderate activity, reaching approximately 25% conversion.

In contrast, the selectivity toward 4-chlorobenzaldehyde was highest for catalysts **5t** and **3t**, both tetranuclear complexes.

Table 7 Conversion and selectivity parameters for 4-chlorobenzyl alcohol to 4-chlorobenzaldehyde oxidation

Temperature	80 °C			
	TBHP in water + 3 mL MeCN			
	Conversion/%		Selectivity/%	
Oxidant Catalyst (0.5 mol%)	120 min	20 min	120 min	20 min
1	56	9	64	83
2	59	13	62	83
3t	42	6	75	89
3	79	26	43	83
3t^{iso}	57	9	64	85
4	77	24	45	81
4^{tert}	74	21	47	85
5t	43	7	75	97
[VO(acac)$_2$]	87	43	29	71
NH_4VO_3	56	14	65	85

Table 8 Conversion and selectivity parameters for 4-nitrobenzyl alcohol to 4-nitrobenzaldehyde oxidation

Temperature	80 °C			
	TBHP in water + 3 mL MeCN			
	Conversion/%		Selectivity/%	
Oxidant Catalyst (0.5 mol%)	120 min	20 min	120 min	20 min
1	54	9	82	98
2	49	12	87	95
3t	88	33	49	79
3	54	17	76	73
3t^{iso}	86	26	53	64
4	87	29	50	92
4^{tert}	63	12	76	88
5t	35	3	92	93
[VO(acac)$_2$]	96	57	27	78
NH_4VO_3	21	4	90	82

After 2 hours, these catalysts maintained selectivities of 75%. Remarkably, after just 20 minutes, selectivity was even higher, 97% for **5t** and 89% for **3t**, indicating their strong ability to favor aldehyde formation in the early stages of the reaction.

An interesting trend emerges when comparing catalyst types over time: tetranuclear catalysts sustain high selectivity throughout the reaction, while polymeric catalysts, although initially selective (within 20 minutes), show a significant decline in aldehyde selectivity as the reaction progresses. For instance, catalysts **3** and **4** display a marked drop, with final selectivities decreasing to approximately 40% after 2 hours. This suggests that polymeric catalysts may be more prone to overoxidation or side reactions during prolonged reaction times.

The reference catalyst [VO(acac)$_2$] demonstrated the highest conversion after 2 hours, reaching 87%, significantly outperforming the other catalysts in **3t^{iso}** terms of substrate oxidation. In comparison, NH_4VO_3 achieved a moderate conversion of 56%, a value comparable to those observed for the polymeric catalysts **1**, **2**, and tetranuclear **3t^{iso}**. However, in terms of selectivity toward 4-chlorobenzaldehyde, [VO(acac)$_2$] performed poorly, exhibiting the lowest selectivity at just 25%, likely due to overoxidation to the corresponding acid or side products. Conversely, NH_4VO_3 offered a more favorable selectivity profile, reaching 65%, which is again comparable to the selectivities observed for catalysts **1**, **2**, and **3t^{iso}**.

The polynuclear catalysts **1**, **2**, **3**, **4**, and **4**^{tert} exhibited moderate to high conversions after 120 minutes of oxidation reaction of 4-nitrobenzyl alcohol. Among them, catalyst **4** demonstrated the highest activity, achieving a conversion of 86.95%, closely approaching the performance of the most active tetranuclear system (**3t^{iso}**). At the early stage (20 minutes), conversion across the polynuclear series was modest, ranging from approximately 9 to 29%.

In terms of aldehyde selectivity, catalysts **1** and **2** stood out, maintaining exceptionally high selectivity values of >95% at 20 minutes, and still performing well after 2 hours (82% and

Open Access Article. Published on 17 February 2026. Downloaded on 4/5/2026 6:35:39 AM.
This article is licensed under a Creative Commons Attribution-NonCommercial 3.0 Unported Licence.

87%, respectively). In contrast, catalysts **3**, **4**, and $\mathbf{4}^{tert}$ showed a marked decline in selectivity over time, likely due to progressive overoxidation to the corresponding acid. For example, catalyst **4** showed a significant drop in selectivity from 92% at 20 minutes to 50% at 120 minutes.

The tetranuclear catalysts **3t** and $\mathbf{3t}^{iso}$ exhibited high conversions after 2 hours (88% and 86%, respectively), ranking among the most active systems tested. However, their aldehyde selectivity decreased with time. **3t** and $\mathbf{3t}^{iso}$ initially showed reasonable selectivity (79% and 64% at 20 minutes), but these values declined to approximately 50% after 2 hours, again suggesting overoxidation during extended reaction periods.

In contrast, tetranuclear catalyst **5t** demonstrated lower conversion (35%) but excellent selectivity, maintaining values above 91% at both 20 and 120 minutes. This indicates a slower but highly chemoselective oxidation process, favoring aldehyde formation and minimizing overoxidation.

Among the reference catalysts, $[VO(acac)_2]$ exhibited the highest overall conversion (96% at 120 min, 57% at 20 min), but the lowest selectivity (27% at 2 h), confirming its tendency to promote complete oxidation, likely to the corresponding acid. On the other hand, NH_4VO_3 was significantly less active (21% conversion at 2 h), but highly selective (90%), resembling the behavior of catalyst **5t**. This makes NH_4VO_3 more suitable for mild and selective oxidation, although its low conversion limits its overall efficiency.

Overall, the trends in conversion and selectivity reported in Tables 6 and 7 reflect the influence of the alkoxo chain length. Short-chain catalysts (**1** and **2**) show moderate conversions due to limited solubility, whereas intermediate linear chains (**3** and **4**) achieve the highest conversions for both substrates, as a result of improved catalyst–substrate interactions. This increase in activity is accompanied by lower selectivity, indicating a greater tendency toward over-oxidation at higher conversion levels. In contrast, the longer-chain catalyst (**5**) and the branched analogues ($\mathbf{3t}^{iso}$, $\mathbf{4}^{tert}$) demonstrate reduced conversions but enhanced selectivities, consistent with increased steric hindrance limiting substrate access to the metal center. These data demonstrate that conversion is maximized at intermediate chain lengths, while selectivity increases with steric bulk, in full agreement with the relationship structure and activity discussed above.

Among the polymeric catalysts, catalyst **3** demonstrated exceptional activity in the oxidation of 4-chlorobenzyl alcohol, with a Cl-TOF of 150.8, positioning it among the most active systems within its class (Fig. 4 and Fig. S13 see SI). In contrast, catalyst **4** exhibited superior performance in the oxidation of 4-nitrobenzyl alcohol, achieving a NO-TOF of 170 and a NO-TON of 172, closely matching the efficiency of the tetranuclear catalyst **3t**. Meanwhile, catalyst $\mathbf{4}^{tert}$ showed good catalyst durability, as evidenced by its high TON values, although its NO-TOF (72) was comparatively lower than that of catalyst **4**, indicating reduced initial activity.

Within the tetranuclear catalyst group, catalyst **3t** emerged as the most effective for 4-nitrobenzyl alcohol oxidation, delivering the highest NO-TOF (197) among all tested systems,

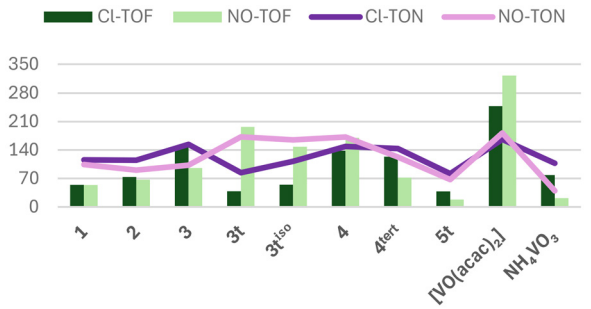

Fig. 4 Comparison of $TOF_{20\ min}$ and TON values for 4-chloro and 4-nitrobenzyl alcohol oxidations.

even surpassing that of $[VO(acac)_2]$. This underscores its suitability for fast, efficient oxidation under mild conditions. Catalyst $\mathbf{3t}^{iso}$ also demonstrated well-balanced catalytic performance, maintaining high activity across both Cl- and NO-substituted alcohols, with consistent TOF and TON values, making it a versatile and robust system.

In contrast, catalyst **5t**, although previously noted for its excellent selectivity, exhibited significantly lower catalytic efficiency, with a NO-TOF of just 18 and NO-TON of 68, indicating slower turnover and limited utility for extended oxidation processes.

The overall mechanism has been discussed previously,[19] above starting with rapid alkoxide–water exchange, forming the hydroxo complex [LVO(OH)], followed by substrate coordination where benzyl alcohol replaces the OH ligand to give $[LVO(OCH_2Ar)]$. Addition of TBHP produces a hydroxo–*tert*-butylperoxo intermediate $[LVO(OH)(OCH_2Ar)(OOtBu)]$, which is poised for the key six-membered transition-state hydrogen transfer from the benzylic CH_2 group. This step is the rate-determining step and leads to a transient species that collapses to release the aldehyde, tBuOH, and regenerate [LVO(OH)], completing the cycle.

Additionally, the basicity of the RO^- influenced by the electronic effects of the solvent, as reflected by alcohol pK_a, is expected to play a relevant role in determining catalytic efficiency. Thus, a more basic alkoxide should be more readily protonated and displaced, thereby facilitating the formation of catalytically active species. Consequently, both the steric requirements and the basicity of the OR ancillary ligand could influence the formation of reactive intermediates. However, due to the similar pK_a values of solvents used (ranging from 15.5 to 17), no significant impact was observed.

Among the reference catalysts, NH_4VO_3 showed moderate activity toward chlorinated substrate (Cl-TOF = 79), but was dramatically less active in the oxidation of nitro-substituted alcohols (NO-TOF = 22). In contrast, $[VO(acac)_2]$ outperformed all catalysts in both substrate classes, with TOF and TON values of 248 and 166 (Cl) and 322 and 182 (NO), respectively. While its high reactivity is undeniable, this catalyst is well-documented for its poor selectivity, which significantly limits its applicability.

This journal is © The Royal Society of Chemistry 2026

Open Access Article. Published on 17 February 2026. Downloaded on 4/5/2026 6:35:39 AM. This article is licensed under a Creative Commons Attribution-NonCommercial 3.0 Unported Licence.

In our previous investigation involving vanadium catalysts derived from (5-methoxy)salicylaldehyde and nicotinic acid hydrazide,[19] tested for the oxidation of 4-nitrobenzyl alcohol, the polymeric catalyst $[VO(5OMeSalNH)(OPr)]_n$ exhibited the highest alcohol conversion, reaching 86% after 120 minutes. However, consistent with the general trend observed for all tested systems, selectivity decreased over time, with the best value at 120 minutes recorded for $[VO(SalNH)(OPr)]_n$ (66%). These findings suggested that bulkier alkoxide ligands, such as propoxyde, may reduce the rate of overoxidation, thereby helping to preserve aldehyde selectivity during extended reaction times. Additionally, $[VO(5OMeSalNH)(OEt)]_n$ showed exceptionally high early-stage selectivity towards aldehyde, achieving 97% at 20 minutes, which is comparable to polymeric catalyst **2**.

Experimental

General details

Commercially available reagents, including ammonium metavanadate, *o*-vanillin, nicotinoyl hydrazide, and solvents, were purchased from Alfa-Aesar or Aldrich and used without further purification. The vanadium precursor $[VO(acac)_2]$,[41] and the hydrazone H_2VanNH[36] were prepared according to literature-reported methods.

Crystalline products obtained from the reactions were used directly for ATR-IR spectroscopy and SCXRD studies. Thermogravimetric analysis (TGA) samples were carefully handled, stored in a desiccator, and kept at −15 °C. Detailed descriptions of characterization techniques, including elemental and thermal analyses, ATR-IR, NMR spectroscopy, PXRD, and SCXRD, along with the corresponding data, are available in the SI.

Synthesis of the metallosupramolecular compounds

Procedure I. Ammonium metavanadate (NH_4VO_3, 0.023 g, 0.20 mmol) was added to a solution of H_2VanNH (0.057 g, 0.21 mmol) in the corresponding alcohol (30 mL). The reaction mixture was refluxed for 3 hours and then cooled to room temperature. The resulting solution was concentrated under reduced pressure (solvent-specific details are outlined in the descriptions of each compound, see below). Upon standing undisturbed at room temperature, dark red-black crystals formed after one week. The crystals were collected by filtration under a dry atmosphere and dried to constant mass in a desiccator maintained at −15 °C.

Procedure II. Bis(acetylacetonato)oxovanadium(IV), $[VO(acac)_2]$ (0.053 g, 0.20 mmol), and H_2VanNH (0.0483 g, 0.20 mmol) were suspended in the appropriate alcohol (30 mL), refluxed for 3 hours and then allowed to cool to room temperature and left to stand undisturbed at room temperature in a sealed flask. After several weeks, dark red-black crystals were collected by filtration under a dry atmosphere and dried to constant mass in a desiccator at −15 °C.

*$[VO(VanNH)(OCH_3)]_n$ (**1**).* The complex was prepared by Procedure I in methanol. The solution was concentrated to about 10 mL after 1 day and left at room temperature. Yield: 0.038 g; 52%. (b) The complex was also prepared by Procedure II in methanol. The solution was concentrated after three weeks to about 20 mL. Yield: 0.011 g; 15%. Anal. calcd for $C_{15}H_{14}N_3O_5V$ (367.23): C, 49.06; H, 3.84; N, 11.44. Found: C, 48.95; H, 3.63; N, 11.29%. TG: CH_3O, 8.31 (calcd 8.45%); V_2O_5, 24.45% (calcd 24.76%). Selected IR data (cm^{-1}): 1608 ($C{=}N)_{imine}$, 1601 (C=N), 1348 ($C{-}O_{hydrazone}$), 1252 ($C{-}O_{phenolato}$), 1034 ($C{-}O_{alkoxo}$), 970 (N–N), 957 (V=O), 740 ($V{-}N_{imine}$), 720 ($V{-}N_{py}$), 604 ($V{-}O_{alkoxo}$), 596 ($V{-}O_{hydrazonato}$), 581 ($V{-}O_{phenolato}$).

*$[VO(VanNH)(OCH_2CH_3)]_n$ (**2**).* The complex was prepared by Procedure I in ethanol and left at room temperature. Yield: 0.049 g; 64%. (b) The complex was also prepared by Procedure II in ethanol. Yield: 0.039 g; 51%. Anal. calcd for $C_{16}H_{16}N_3O_5V$ (381.26): C, 50.40; H, 4.23; N, 11.02. Found: C, 50.26; H, 4.18; N, 10.88%. TG: C_2H_5O, 11.64 (calcd 11.82%); V_2O_5, 23.65% (calcd 23.85%). Selected IR data (cm^{-1}): 1615 ($C{=}N)_{imine}$, 1610, 1592 (C=N), 1351 ($C{-}O_{hydrazone}$), 1252 ($C{-}O_{phenolato}$), 1033 ($C{-}O_{alkoxo}$), 961 (N–N), 956 (V=O), 740 ($V{-}N_{imine}$), 700 ($V{-}N_{py}$), 604 ($V{-}O_{alkoxo}$), 595 ($V{-}O_{hydrazonato}$), 581 ($V{-}O_{phenolato}$).

*$[VO(VanNH)(OC_3H_7)]_4$ (**3t**).* The complex was prepared by Procedure I in *n*-propanol. The solution was placed in the refrigerator the following day. Yield: 0.034 g; 43%. (b) The complex was also prepared by Procedure II in *n*-propanol. The solution was concentrated to about 20 mL and placed in the refrigerator. Yield: 0.042 g; 53%. Anal. calcd for $C_{17}H_{18}N_3O_5V$ (1581.132): C, 51.65; H, 4.59; N, 10.63. Found: C, 51.52; H, 4.45; N, 10.48%. TG: C_3H_7O, 14.66 (calcd 14.95%); V_2O_5, 22.80% (calcd 23.01%). Selected IR data (cm^{-1}): 1611 ($C{=}N)_{imine}$, 1599 (C=N), 1348 ($C{-}O_{hydrazone}$), 1255 ($C{-}O_{phenolato}$), 1032 ($C{-}O_{alkoxo}$), 970 (N–N), 958 (V=O), 733 ($V{-}N_{imine}$), 717 ($V{-}N_{py}$), 602 ($V{-}O_{alkoxo}$), 596 ($V{-}O_{hydrazonato}$), 587 ($V{-}O_{phenolato}$).

*$[VO(VanNH)(OC_3H_7)]_n$ (**3α**).* The complex was prepared by Procedure I in *n*-propanol. The solution was concentrated to about 15 mL after 1 day and left at room temperature. Yield: 0.022 g; 28%. Anal. calcd for $C_{17}H_{18}N_3O_5V$ (395.283): C, 51.65; H, 4.59; N, 10.63. Found: C, 51.52; H, 4.41; N, 10.44%. TG: C_3H_7O, 14.65 (calcd 14.95%); V_2O_5, 22.72% (calcd 23.01%). Selected IR data (cm^{-1}): 1615 ($C{=}N)_{imine}$, 1608, 1597 (C=N), 1348 ($C{-}O_{hydrazone}$), 1257 ($C{-}O_{phenolato}$), 1032 ($C{-}O_{alkoxo}$), 971 (N–N), 957 (V=O), 730 ($V{-}N_{imine}$), 721 ($V{-}N_{py}$), 602 ($V{-}O_{alkoxo}$), 594 ($V{-}O_{hydrazonato}$), 587 ($V{-}O_{phenolato}$).

*$[VO(VanNH)(OC_3H_7)]_n$ (**3β**).* The complex was prepared by Procedure I in *n*-propanol. The reaction mixture was heated, then evaporated to about 10 mL without disturbing the flask, and left at room temperature. Yield: 0.038 g; 48%. Anal. calcd for $C_{17}H_{18}N_3O_5V$ (395.283): C, 51.65; H, 4.59; N, 10.63. Found: C, 51.45; H, 4.42; N, 10.46%. Found: C, 51.39; H, 4.33; N, 10.31%. TG: C_3H_7O, 14.54 (calcd 14.95%); V_2O_5, 22.71% (calcd 23.01%). Selected IR data (cm^{-1}): 1616 ($C{=}N)_{imine}$, 1608, 1598 (C=N), 1350 ($C{-}O_{hydrazone}$), 1255 ($C{-}O_{phenolato}$), 1032 ($C{-}O_{alkoxo}$), 962 (N–N), 959 (V=O), 734 ($V{-}N_{imine}$), 717 ($V{-}N_{py}$), 600 ($V{-}O_{alkoxo}$), 583 ($V{-}O_{hydrazonato}$), 566 ($V{-}O_{phenolato}$).

*$[VO(VanNH)\{OCH(CH_3)_2\}]_4$ (**3t^{iso}**).* The complex was prepared in isopropanol by Procedure I. The solution was concentrated

Open Access Article. Published on 17 February 2026. Downloaded on 4/5/2026 6:35:39 AM. This article is licensed under a Creative Commons Attribution-NonCommercial 3.0 Unported Licence.

to about 10 mL after 1 day and left at room temperature. Yield: 0.066 g; 83%. Anal. calcd for $C_{17}H_{18}N_3O_5V$ (1581.132): C, 51.65; H, 4.59; N, 10.63. Found: C, 51.49; H, 4.46; N, 10.49%. TG: C_3H_7O, 14.88 (calcd 14.95%); V_2O_5, 22.71% (calcd 23.01%). Selected IR data (cm^{-1}): 1615 $(C{=}N)_{imine}$, 1610, 1594 (C=N), 1352 $(C{-}O_{hydrazone})$, 1256 $(C{-}O_{phenolato})$, 1029 $(C{-}O_{alkoxo})$, 971 (N–N), 956 (V=O), 735 $(V{-}N_{imine})$, 718 $(V{-}N_{py})$, 601 $(V{-}O_{alkoxo})$, 590 $(V{-}O_{hydrazonato})$, 575 $(V{-}O_{phenolato})$.

*[VO(VanNH)(OC$_4$H$_9$)]$_n$ (**4α**).* The complex was prepared by Procedure II in *n*-butanol and left at room temperature. Yield: 0.006 g; 7%. Anal. calcd for $C_{18}H_{20}N_3O_5V$ (409.31): C, 52.82; H, 4.93; N, 10.27. Found: C, 52.73; H, 4.69; N, 10.15%. TG: C_4H_9O, 17.58 (calcd 17.86%); V_2O_5, 22.03% (calcd 22.22%). Selected IR data (cm^{-1}): 1616 $(C{=}N)_{imine}$, 1612, 1594 (C=N), 1357 $(C{-}O_{hydrazone})$, 1253 $(C{-}O_{phenolato})$, 1030 $(C{-}O_{alkoxo})$, 971 (N–N), 959 (V=O), 738 $(V{-}N_{imine})$, 719 $(V{-}N_{py})$, 600 $(V{-}O_{alkoxo})$, 580 $(V{-}O_{hydrazonato})$, 568 $(V{-}O_{phenolato})$.

*[VO(VanNH)(OC$_4$H$_9$)]$_n$ (**4β**).* The complex was prepared by Procedure I in *n*-butanol. The solution was concentrated to about 10 mL after 1 day and left at room temperature. Yield: 0.059 g; 72%. Anal. calcd for $C_{18}H_{20}N_3O_5V$ (409.31): C, 52.82; H, 4.93; N, 10.27. Found: C, 52.74; H, 4.79; N, 10.12%. TG: C_4H_9O, 17.58 (calcd 17.86%); V_2O_5, 21.99% (calcd 22.22%). Selected IR data (cm^{-1}): 1616 $(C{=}N)_{imine}$, 1612, 1594 (C=N), 1357 $(C{-}O_{hydrazone})$, 1253 $(C{-}O_{phenolato})$, 1030 $(C{-}O_{alkoxo})$, 971 (N–N), 959 (V=O), 738 $(V{-}N_{imine})$, 719 $(V{-}N_{py})$, 600 $(V{-}O_{alkoxo})$, 580 $(V{-}O_{hydrazonato})$, 568 $(V{-}O_{phenolato})$.

*[VO(VanNH){OC(CH$_3$)$_3$}]$_n$ (**4^{tert}**).* The complex was prepared according to Procedure I in *tert*-butanol under reflux for 6 hours. The solution was concentrated to about 10 mL after 1 day and left at room temperature. Yield: 0.072 g; 88%. Anal. calcd for $C_{18}H_{20}N_3O_5V$ (409.31): C, 52.82; H, 4.93; N, 10.27. Found: C, 52.78; H, 4.73; N, 10.11%. TG: C_4H_9O, 17.57 (calcd 17.86%); V_2O_5, 21.95% (calcd 22.22%). Selected IR data (cm^{-1}): 1615 $(C{=}N)_{imine}$, 1612, 1594 (C=N), 1349 $(C{-}O_{hydrazone})$, 1254 $(C{-}O_{phenolato})$, 1033 $(C{-}O_{alkoxo})$, 975 (N–N), 959 (V=O), 735 $(V{-}N_{imine})$, 723 $(V{-}N_{py})$, 599 $(V{-}O_{alkoxo})$, 587 $(V{-}O_{hydrazonato})$, 578 $(V{-}O_{phenolato})$.

*[VO(VanNH)(OC$_5$H$_{11}$)]$_4$ (**5tβ**).* The complex was prepared by Procedure I in *n*-pentanol. The solution was concentrated to about 5 mL after 1 day. Yield: 0.015 g; 17%. Anal. calcd for $C_{19}H_{22}N_3O_5V$ (423.336): C, 53.91; H, 5.24; N, 9.93. Found: C, 53.78; H, 5.13; N, 9.69%. TG: $C_5H_{11}O$, 20.24 (calcd 20.58%); V_2O_5, 21.17% (calcd 21.48%). Selected IR data (cm^{-1}): 1616 $(C{=}N)_{imine}$, 1596 (C=N), 1350 $(C{-}O_{hydrazone})$, 1262 $(C{-}O_{phenolato})$, 1043 $(C{-}O_{alkoxo})$, 970 (N–N), 962 (V=O), 750 $(V{-}N_{imine})$, 708 $(V{-}N_{py})$, 602 $(V{-}O_{alkoxo})$, 580 $(V{-}O_{hydrazonato})$, 571 $(V{-}O_{phenolato})$.

Quantum chemical calculations

Optimizations of geometries for all computed complexes were performed using the hybrid functional B3LYP[42] with the D3 version of Grimme's dispersion[43] and Becke–Johnson dumping in combination with the 6-31G(d)[44,45] basis set. Initial geometries were taken from crystallographically determined structures. To confirm that the obtained geometries were local minima, harmonic frequency calculations were performed.[46,47] The standard Gibbs energies of formation were calculated at T = 298.15 K and p = 101 325 Pa. Strengths of the intramolecular interactions were estimated by the calculation of relative differences in the standard enthalpies, entropies and Gibbs energies of binding $\Delta_b G°$ and $\Delta\Delta_f G°$.[48] All quantum chemical calculations were carried out using the Gaussian 16 program package.[49]

Catalysis

The catalytic oxidation of 4-nitrobenzyl alcohol and 4-chlorobenzyl alcohol was performed using vanadium-based coordination complexes as catalysts in a magnetically stirred, three-necked 50 mL round-bottom flask equipped with a reflux condenser. The reaction system comprised 4-nitrobenzyl alcohol or 4-chlorobenzyl alcohol (3.30 mmol), an oxidant TBHP in aqueous medium (6.60 mmol), acetophenone (3.43 mmol) as an internal standard, the catalyst (0.0165 mmol) and 3 mL of acetonitrile. Reactions were conducted at 80 °C under continuous stirring for two hours. At defined time intervals, aliquots were withdrawn, immediately diluted with acetonitrile, and subjected to gas chromatographic (GC) analysis.

Conclusions

A series of tetrameric and polymeric coordination-driven assemblies was obtained depending on reaction conditions and the auxiliary alkoxide ligands. Although tetramers are generally more stable than monomers, comparison with chain models shows that the polymers featuring alternating '*syn*' and '*anti*' units have significantly more exergonic binding energies, making them thermodynamically preferred over tetramers across the alkoxide series. This stabilization arises primarily from its higher exothermic binding enthalpy, which exceeds the entropic contribution associated with the akoxide chain length. Conversely, the polymeric type with the *anti*-motif is favored for longer alkoxo ligands. The observed structural diversity, reflects a delicate balance of electronic, steric, and packing effects that determine which species crystallize.

The oxidation of 4-chlorobenzyl and 4-nitrobenzyl alcohols revealed apparent performance differences among vanadium catalysts. Polymers **3**, **4**, and **4^{tert}** delivered the highest conversions (up to 79–87% for **3** and **4**), though their selectivity dropped significantly over time due to overoxidation. In contrast, polymers **1** and **2** maintained excellent selectivity in the nitro-series (>95% at 20 min).

Among tetranuclear complexes, **3t** and **3t^{iso}** showed high activity (up to 88% conversion for **3t**), with **3t** giving the highest $TOF_{20\ min}$ (197) of all tested systems. Tetranuclear **5t**, although less active (35% conversion), consistently showed exceptionally high selectivity (>91% at both time points), making it the most selective catalyst. Overall, the results highlight a fundamental trade-off: highly active catalysts (**3**, **4**, **3t**, $[VO(acac)_2]$) tend to lose selectivity, whereas highly selective systems (**1**, **2**, **5t**, NH_4VO_3) operate more slowly. Catalyst nucle-

 This journal is © The Royal Society of Chemistry 2026

Open Access Article. Published on 17 February 2026. Downloaded on 4/5/2026 6:35:39 AM. This article is licensed under a Creative Commons Attribution-NonCommercial 3.0 Unported Licence.

arity and alkoxo ligand structure strongly influence this balance, offering key design principles for future vanadium oxidation catalysts.

Author contributions

Edi Topić: investigation, writing – original draft preparation, writing – review and editing. Josipa Sarjanović: formal analysis, data curation. Dino Kuzman: investigation and formal analysis. Andrea Cocut: formal analysis, data curation. Tomica Hrenar: investigation, supervision, writing – original draft preparation, writing – review and editing. Jana Pisk: investigation, supervision, writing – original draft preparation. Višnja Vrdoljak: conceptualization, funding acquisition, investigation, writing – original draft preparation, visualization, review and editing.

Conflicts of interest

There are no conflicts to declare.

Data availability

The data supporting this article have been included as part of the supplementary information (SI). Supplementary information: (1) schemes, (2) experimental and crystallographic data for compounds, (3) selected bond lengths, (4) asymmetric unit and packing of molecules in the crystal structure; (5) powder diffraction patterns, (6) ATR-IR spectra, (7) NMR spectra (8) TGA curves, (9) kinetic profiles. See DOI: https://doi.org/10.1039/d5dt03088a.

CCDC 2518093 (**1**), 2518094 (**2**), 2518095 (**3t**), 2518096 (**3α**), 2518097 (**3β**), 2518098 (**3t^{iso}**), 2518099 (**4α**), 25180100 (**4β**), 25180101 (**4^{tert}**), 25180102 (**5tα**) and 2518103 (**5tβ**) contain the supplementary crystallographic data for this paper.[50a–k]

Acknowledgements

This work was supported by the Croatian Science Foundation under the project number HRZZ-IP-2022-10-7368. We acknowledge the support of project CIuK co-financed by the Croatian Government and the European Union through the European Regional Development Fund-Competitiveness and Cohesion Operational Programme (Grant KK.01.1.1.02.0016.).

References

1 R. R. Langeslay, D. M. Kaphan, C. L. Marshall, P. C. Stair, A. P. Sattelberger and M. Delferro, Catalysis with Supported Molecular Vanadium Complexes, *Chem. Rev.*, 2019, **119**, 2128–2191, DOI: 10.1021/acs.chemrev.8b00245.

2 M. Sutradhar, M. V. Kirillova, M. F. C. Guedes da SIlva, L. M. D. R. S. Martins and A. J. L. Pombeiro, A Hexanuclear Mixed-Valence Oxovanadium(IV,V) Complex as a Highly Efficient Alkane Oxidation Catalyst, *Inorg. Chem.*, 2012, **51**, 11229–11238, DOI: 10.1021/ic3017062.

3 X. Xu, H. Wang, C.-H. Tan and X. Ye, Applications of Vanadium, Niobium, and Tantalum Complexes in Organic and Inorganic Synthesis, *ACS Org. Inorg. Au*, 2023, **3**, 74–91, DOI: 10.1021/acsorginorgau.2c00053.

4 I. Gryca, K. Czerwińska, B. Machura, A. Chrobok, L. S. Shul'pina, M. L. Kuznetsov, D. S. Nesterov, Y. N. Kozlov, A. L. Pombeiro, I. A. Varyan and G. B. Shul'pin, High Catalytic Activity of Vanadium Complexes in Alkane Oxidations with Hydrogen Peroxide: An Effect of 8-Hydroxyquinoline Derivatives as Noninnocent Ligands, *Inorg. Chem.*, 2018, **57**, 1824–1838, DOI: 10.1021/acs.inorgchem.7b02684.

5 A. G. J. Ligtenbarg, R. Hage and B. L. Feringa, Catalytic, oxidation by vanadium complexes, *Coord. Chem. Rev.*, 2003, **237**, 89–101, DOI: 10.1016/S0010-8545(02)00308-9.

6 N. Mizuno and K. Kamata, Catalytic oxidation of hydrocarbons with hydrogen peroxide by vanadium-based molecular catalysts, *Coord. Chem. Rev.*, 2011, **255**, 2358–2370, DOI: 10.1016/j.ccr.2011.01.041.

7 F. Cavani, N. Ballarini and A. Cericola, Oxidative dehydrogenation of ethane and propane: how far from commercial implementation?, *Catal. Today*, 2007, **127**, 113–131, DOI: 10.1016/j.cattod.2007.05.009.

8 S. Takizawa, T. Katayama and H. Sasai, Dinuclear chiral vanadium catalysts for oxidative coupling of 2-naphthols via a dual activation mechanism, *Chem. Commun.*, 2008, 4113–4122, DOI: 10.1039/B806016A.

9 C. Bolm, Vanadium-catalyzed asymmetric oxidations, *Coord. Chem. Rev.*, 2003, **237**, 245–256, DOI: 10.1016/S0010-8545(02)00249-7.

10 I. Correia, P. Adão, S. Roy, M. Wahba, C. Matos, M. R. Maurya, F. Marques, F. R. Pavan, C. Q. F. Leite and F. Avecilla, Hydroxyquinoline derived vanadium(IV and V) and copper(II) complexes as potential anti-tuberculosis and anti-tumor agents, *J. Inorg. Biochem.*, 2014, **141**, 83–93, DOI: 10.1016/j.jinorgbio.2014.07.019.

11 M. Mohanty, S. K. Maurya, A. Banerjee, S. A. Patra, M. R. Maurya, A. Crochet, K. Brzeziński and R. Dinda, *In vitro* cytotoxicity and catalytic evaluation of dioxidovanadium (V) complexes in an azohydrazone ligand environment, *New J. Chem.*, 2019, **43**, 17680–17695, DOI: 10.1039/C9NJ01815H.

12 J. Zhu, X. Chen, A. Q. Thang, F.-L. Li, D. Chen, H. Geng, X. Rui and Q. Yan, Vanadium-based metal–organic frameworks and their derivatives: synthesis, properties, and applications, *Small Methods*, 2022, **6**, 2200911, DOI: 10.1002/smm2.1091.

13 F. Farzinpour, A. A. Ensafi, K. Z. Mousaabadi and B. Rezaei, Synthesis of vanadium metal-organic framework, characterization, and study of electrochemical properties for use in supercapacitors and oxygen evolution reaction, *Fuel*, 2023, **341**, 127724, DOI: 10.1016/j.fuel.2023.127724.

Open Access Article. Published on 17 February 2026. Downloaded on 4/5/2026 6:35:39 AM. This article is licensed under a Creative Commons Attribution-NonCommercial 3.0 Unported Licence.

14 D. Dragancea, N. Talmaci, S. Shova, G. Novitchi, D. Darvasiová, P. Rapta, M. Breza, M. Galanski, J. Kožíšek, N. M. R. Martins, L. M. D. R. S. Martins, A. J. L. Pombeiro and V. B. Arion, Vanadium(v) Complexes with Substituted 1,5-bis(2-hydroxybenzaldehyde)carbohydrazones and their Use As Catalyst Precursors in Oxidation of Cyclohexane, *Inorg. Chem.*, 2016, **55**, 9187–9203, DOI: 10.1021/acs.inorgchem.6b01011.

15 M. R. Maurya, M. Nandi, P. K. Chaudhary, S. Singh, F. Avecilla, R. Prasad and K. Ghosh, Catalytic, antifungal, and antiproliferative activity studies of a new family of mononuclear [VVO]/[VVO_2] complexes, *Inorg. Chem.*, 2024, **63**, 714–729, DOI: 10.1021/acs.inorgchem.3c03665.

16 H. Hosseini Monfared, V. Abbasi, A. Rezaei and M. Ghiaci, A heterogenized vanadium oxo-aroylhydrazone catalyst for efficient and selective oxidation of hydrocarbons with hydrogen peroxide, *Transition Met. Chem.*, 2012, **37**, 85–92, DOI: 10.1007/s11243-011-9561-4.

17 E. Topić, J. Sarjanović, D. Musija, M. Mandarić, T. Hrenar, J. Pisk and V. Vrdoljak, High-valent oxovanadium metallosupramolecular species as catalysts for the oxidation of benzyl alcohol derivatives, *RSC Adv.*, 2025, **15**, 3547–3561, DOI: 10.1039/D4RA09073J.

18 E. Topić, J. Sarjanović, D. Musija, M. Mandarić, A. Cocut, T. Hrenar, D. Agustin, J. Pisk and V. Vrdoljak, Influence of ancillary ligands on the formation and functionality of oxovanadium(v) metallosupramolecular assemblies: advanced computational and catalytic analysis, *Dalton Trans.*, 2025, **54**, 5532–5545, DOI: 10.1039/D5DT00105F.

19 D. Kuzman, J. Sarjanović, M. Mandarić, M. Cindrić, D. Agustin, J. Pisk and V. Vrdoljak, Tailored pincer ligand-based oxidovanadium complexes of varying nuclearity and geometry: Catalytic performances and computational insights, *Inorg. Chem. Commun.*, 2026, **183**(2), 115817, DOI: 10.1016/j.inoche.2025.115817.

20 V. Vrdoljak, M. Mandarić, T. Hrenar, I. Đilović, J. Pisk, G. Pavlović, M. Cindrić and D. Agustin, Geometrically constrained molybdenum(vi) metallosupramolecular architectures: conventional Synthesis versus vapor and thermally induced solid-state structural transformations, *Cryst. Growth Des.*, 2019, **19**, 3000–3011, DOI: 10.1021/acs.cgd.9b00231.

21 J. Pisk, D. Agustin and V. Vrdoljak, Tetranuclear molybdenum(vi) hydrazonato epoxidation (pre)catalysts: Is water always the best choice?, *Catal. Commun.*, 2020, **142**, 106027, DOI: 10.1016/j.catcom.2020.106027.

22 S. Leininger, B. Olenyuk and P. J. Stang, Self-assembly of discrete cyclic nanostructures mediated by transition metals, *Chem. Rev.*, 2000, **100**, 853–908, DOI: 10.1021/cr9601324.

23 T. R. Cook and P. J. Stang, Recent developments in the preparation and chemistry of metallacycles and metallacages via coordination, *Chem. Rev.*, 2015, **115**, 7001–7045, DOI: 10.1021/cr5005666.

24 J.-P. Zhang, X.-C. Huang and X.-M. Chen, Supramolecular isomerism in coordination polymers, *Chem. Soc. Rev.*, 2009, **38**, 2385–2396, DOI: 10.1039/B900317G.

25 P. I. da S. Maia, V. M. Deflon, E. J. de. Souza, E. Garcia, G. F. de. Sousa, A. A. Batista, A. T. de. Figueiredo and E. Niquet, Biomimetic oxovanadium(iv) and (V) complexes with a tridentate (N,N,O)-donor hydrazonic ligand. Two X-ray crystal structure modifications of (2-acetylpyridine-, benzoylhydrazonato)dioxovanadium(v), *Transition Met. Chem.*, 2005, **30**, 404–410, DOI: 10.1007/s11243-004-6972-5.

26 M. R. P. Kurup, E. B. Seena and M. Kuriakose, Synthesis, spectral and structural studies of oxovanadium(IV/V) complexes derived from 2-hydroxyacetophenone-3-hydroxy-2-naphthoylhydrazone: polymorphs of oxovanadium(v) complex [VOL(OCH_3)], *Struct. Chem.*, 2010, **21**, 599–605, DOI: 10.1007/s11224-010-9589-7.

27 Y. Jin and M. S. Lah, Polymorphism Driven by π–π Stacking and van der Waals Interactions: Preparation and Characterization of Polymorphic Vanadium Crystals of [VVO(Hacshz)(OEt)] and [VIV(Hacshz)$_2$], *Eur. J. Inorg. Chem.*, 2005, **2005**, 4944–4952, DOI: 10.1002/ejic.200500222.

28 N. Heydari, R. Bikas, M. Shaterian, M. S. Krawczyk and T. Lis, Investigation of the substituent effects on the oxidation of styrene derivatives by silica–supported heterogeneous oxidovanadium(v) coordination compound, *Appl. Organomet. Chem.*, 2023, **37**, e6976, DOI: 10.1002/aoc.6976.

29 M. Rubčić, D. Milić, G. Pavlović and M. Cindrić, Conformational Diversity of Thiosemicarbazonatovanadium(v) Complexes in the Solid State: From Polymorphism to Isostructurality, *Cryst. Growth Des.*, 2011, **11**, 5227–5240, DOI: 10.1021/cg200466b.

30 E. Salojärvi, A. Peuronen, M. Lahtinen, H. Huhtinen, L. S. Vlasenko, M. Lastusaari and A. Lehtonen, Series of Near-IR-Absorbing Transition Metal Complexes with Redox Active Ligands, *Molecules*, 2020, **25**, 2531, DOI: 10.3390/molecules25112531.

31 L. M. Mokry and C. J. Carrano, Steric control of vanadium (v) coordination geometry: a mononuclear structural model for transition-state-analog RNase inhibitors, *Inorg. Chem.*, 1993, **32**, 6119–6121, DOI: 10.1021/ic00078a036.

32 B. Baruah, S. P. Rath and A. Chakravorty, A Novel Pentacoordinated Dioxovanadium(v) Salicylaldiminate: Solvent Specific Crystallization of Dimorphs with Contrasting Coordination Geometries, Ligand Conformations and Supramolecular Architectures, *Eur. J. Inorg. Chem.*, 2004, **2004**, 1873–1878, DOI: 10.1002/ejic.200300612.

33 M. A. Fik, A. Gorczyński, M. Kubicki, Z. Hnatejko, A. Wadas, P. J. Kulesza, A. Lewińska, M. Giel-Pietraszuk, E. Wyszko and V. Patroniak, New vanadium complexes with 6,6″-dimethyl-2,2′:6′,2″-terpyridine in terms of structure and biological properties, *Polyhedron*, 2015, **97**, 83–93, DOI: 10.1016/j.poly.2015.05.021.

34 M. Motevalli, D. Shah, S. A. A. Shah and A. C. Sullivan, A novel route to oxovanadium halides. Synthesis and X-ray structures of $VOCl_2$·3Py and VO_2Cl·2Py, *Polyhedron*, 1996, **15**, 2387–2395, DOI: 10.1016/0277-5387(95)00509-9.

35 W. Chen, T. Suenobu and S. Fukuzumi, A Vanadium Porphyrin with Temperature-Dependent Phase Transformation: Synthesis, Crystal Structures,

 This journal is © The Royal Society of Chemistry 2026

Open Access Article. Published on 17 February 2026. Downloaded on 4/5/2026 6:35:39 AM. This article is licensed under a Creative Commons Attribution-NonCommercial 3.0 Unported Licence.

Supramolecular Motifs and Properties, *Chem. – Asian J.*, 2011, **6**, 1416–1422, DOI: 10.1002/asia.201000822.

36 J. Pisk, T. Hrenar, M. Rubčić, G. Pavlović, V. Damjanović, J. Lovrić, M. Cindrić and V. Vrdoljak, Comparative studies on conventional and solvent-free synthesis toward hydrazones: application of PXRD and chemometric data analysis in mechanochemical reaction monitoring, *CrystEngComm*, 2018, **20**, 1804–1817, DOI: 10.1039/C7CE02136D.

37 K. M. Steed and J. W. Steed, Packing Problems: High Z′ Crystal Structures and Their Relationship to Cocrystals, Inclusion Compounds, and Polymorphism, *Chem. Rev.*, 2015, **115**, 2895–2933, DOI: 10.1021/cr500564z.

38 J.-P. Zhang, X.-C. Huang and X.-M. Chen, Supramolecular isomerism in coordination polymers, *Chem. Soc. Rev.*, 2009, **38**, 2385–2396, DOI: 10.1039/B900317G.

39 D. C. Crans, H. Chen and R. A. Felty, Synthesis and reactivity of oxovanadium(v) trialkoxides of bulky and chiral alcohols, *J. Am. Chem. Soc.*, 1992, **114**, 4543–4550, DOI: 10.1021/ja00038a015.

40 J. Döbler, M. Pritzsche and J. Sauer, Oxidation of Methanol to Formaldehyde on Supported Vanadium Oxide Catalysts Compared to Gas Phase Molecules, *J. Am. Chem. Soc.*, 2005, **127**, 10861–10868, DOI: 10.1021/ja051720e.

41 B. E. Bryant, W. C. Fernelius, D. H. Busch, R. C. Stoufer and W. Stratton, Vanadium(IV) Oxy(acetylacetonate), in *Inorganic Syntheses*, ed. T. Moeller, John Wiley & Sons, Inc, 1957, vol. 5, pp. 113–116. DOI: 10.1002/9780470132364.ch$_3$0.

42 (*a*) C. Lee, W. Yang and R. G. Parr, Development of the Colle-Salvetti correlation-energy formula into a functional of the electron density, *Phys. Rev. B: Condens. Matter Mater. Phys.*, 1998, **37**, 785, DOI: 10.1103/PhysRevB.37.785; (*b*) R. Peverati and D. G. Truhlar, Screened-exchange density functionals with broad accuracy for chemistry and solid-state physics, *Phys. Chem. Chem. Phys.*, 2012, **14**, 16187, DOI: 10.1039/C2CP42576A.

43 S. Grimme, S. Ehrlich and L. Goerigk, Effect of the damping function in dispersion corrected density functional theory, *J. Comput. Chem.*, 2011, **32**, 1456–1465, DOI: 10.1002/jcc.21759.

44 V. A. Rassolov, M. A. Ratner, J. A. Pople, P. C. Redfern and L. A. Curtiss, 6-31G* basis set for third-row atoms, *J. Comput. Chem.*, 2001, **22**, 976–984, DOI: 10.1002/jcc.1058.

45 (*a*) F. Weigend and R. Ahlrichs, Balanced basis sets of split valence, triple zeta valence and quadruple zeta valence quality for H to Rn: Design and assessment of accuracy, *Phys. Chem. Chem. Phys.*, 2005, **7**, 3297–3305, DOI: 10.1039/B508541A; (*b*) F. Weigend, Accurate Coulomb-fitting basis sets for H to Rn, *Phys. Chem. Chem. Phys.*, 2006, **8**, 1057–1065, DOI: 10.1039/B515623H.

46 T. Hrenar, I. Primožič, D. Fijan and M. Majerić Elenkov, Conformational analysis of spiro-epoxides by principal component analysis of molecular dynamics trajectories, *Phys. Chem. Chem. Phys.*, 2017, **19**, 31706–31713, DOI: 10.1039/c7cp05600a.

47 I. Primožič, T. Hrenar, K. Baumann, L. Krišto, I. Križić and S. Tomić, Mechanochemical and Conformational Study of N-heterocyclic Carbonyl-Oxime Transformations, *Croat. Chem. Acta*, 2014, **87**, 153–160, DOI: 10.5562/cca2476.

48 Z. Spahić, T. Hrenar and I. Primožič, Polytopal Rearrangement Governing Stereochemistry of Bicyclic Oxime Ether Synthesis, *Int. J. Mol. Sci.*, 2022, **23**, 12331, DOI: 10.3390/ijms232012331.

49 M. J. Frisch, G. W. Trucks, H. B. Schlegel, G. E. Scuseria, M. A. Robb, J. R. Cheeseman, G. Scalmani, V. Barone, G. A. Petersson, H. Nakatsuji, X. Li, M. Caricato, A. V. Marenich, J. Bloino, B. G. Janesko, R. Gomperts, B. Mennucci, H. P. Hratchian, J. V. Ortiz, A. F. Izmaylov, J. L. Sonnenberg, D. Williams-Young, F. Ding, F. Lipparini, F. Egidi, J. Goings, B. Peng, A. Petrone, T. Henderson, D. Ranasinghe, V. G. Zakrzewski, J. Gao, N. Rega, G. Zheng, W. Liang, M. Hada, M. Ehara, K. Toyota, R. Fukuda, J. Hasegawa, M. Ishida, T. Nakajima, Y. Honda, O. Kitao, H. Nakai, T. Vreven, K. Throssell, J. A. Montgomery Jr., J. E. Peralta, F. Ogliaro, M. J. Bearpark, J. J. Heyd, E. N. Brothers, K. N. Kudin, V. N. Staroverov, T. A. Keith, R. Kobayashi, J. Normand, K. Raghavachari, A. P. Rendell, J. C. Burant, S. S. Iyengar, J. Tomasi, M. Cossi, J. M. Millam, M. Klene, C. Adamo, R. Cammi, J. W. Ochterski, R. L. Martin, K. Morokuma, O. Farkas, J. B. Foresman and D. J. Fox, *Gaussian 16, Revision A.03*, Gaussian, Inc., Wallingford CT, 2016.

50 (*a*) CCDC 2518093: Experimental Crystal Structure Determination, 2026, DOI: 10.5517/ccdc.csd.cc2qj8tc; (*b*) CCDC 2518094: Experimental Crystal Structure Determination, 2026, DOI: 10.5517/ccdc.csd.cc2qj8vd; (*c*) CCDC 2518095: Experimental Crystal Structure Determination, 2026, DOI: 10.5517/ccdc.csd.cc2qj8wf; (*d*) CCDC 2518096: Experimental Crystal Structure Determination, 2026, DOI: 10.5517/ccdc.csd.cc2qj8xg; (*e*) CCDC 2518097: Experimental Crystal Structure Determination, 2026, DOI: 10.5517/ccdc.csd.cc2qj8yh; (*f*) CCDC 2518098: Experimental Crystal Structure Determination, 2026, DOI: 10.5517/ccdc.csd.cc2qj8zj; (*g*) CCDC 2518099: Experimental Crystal Structure Determination, 2026, DOI: 10.5517/ccdc.csd.cc2qj90l; (*h*) CCDC 2518100: Experimental Crystal Structure Determination, 2026, DOI: 10.5517/ccdc.csd.cc2qj91m; (*i*) CCDC 2518101: Experimental Crystal Structure Determination, 2026, DOI: 10.5517/ccdc.csd.cc2qj92n; (*j*) CCDC 2518102: Experimental Crystal Structure Determination, 2026, DOI: 10.5517/ccdc.csd.cc2qj93p; (*k*) CCDC 2518103: Experimental Crystal Structure Determination, 2026, DOI: 10.5517/ccdc.csd.cc2qj94q.